Nanoindentation analysis as a two-dimensional tool for mapping the mechanical properties of complex surfaces

Citation: Randall, Nicholas X., Matthieu Vandamme, and Franz-Josef Ulm. "Nanoindentation analysis as a two-dimensional tool for mapping the mechanical properties of complex surfaces." Journal of Materials Research 24 (2011): 679-690. © Materials Research Society 2009.

As Published: http://dx.doi.org/10.1557/jmr.2009.0149

Publisher: Materials Research Society

Persistent URL: http://hdl.handle.net/1721.1/66546

Version: Final published version: final published article, as it appeared in a journal, conference proceedings, or other formally published context

High Throughput Nanoindentation

The grid indentation technique has recently been developed as a two-dimensional mapping tool for examining the properties of constituent phases independently of each other. This approach relies on large arrays of nanoindentations and statistical analysis of the resulting data.

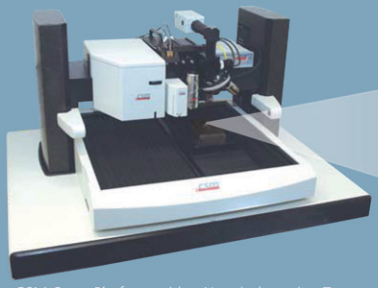

CSM Open Platform with a Nanoindentation Tester, Nano Scratch, AFM and Optical Video Microscope

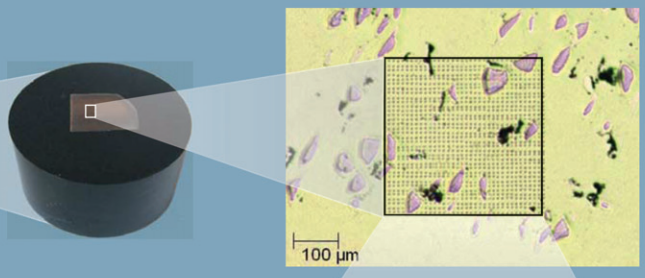

Ti64-10TiC alloy section with TiC particules embedded in a Ti matrix

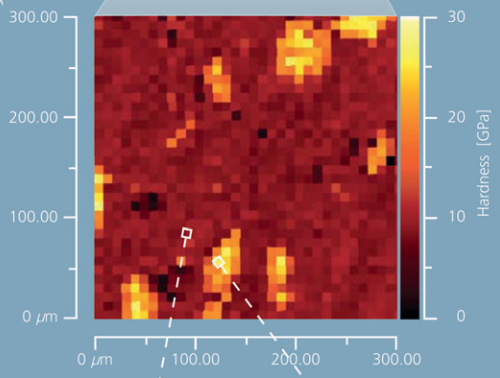

//// 5 EASY STEPS TO CONSTITUENT PROPERTIES

STEP 1 : Place polished and mounted sample section on Nanoindentation Tester

STEP 2 : Run a 2500 indent matrix on a preselected area

STEP 3 : Plot mechanical property (hardness, modulus, creep, etc.) as a 2D map

STEP 4 : Plot data as histogram to extract properties of each phase present

STEP 5 : Calculate volume fractions of phases present

//// ADVANTAGES OF CSM INSTRUMENTS NANOINDENTATION TESTERS

> Full automation allows >1000 indent matrix

> Top-referencing system means that the indenter never goes "out of range"

> Ultra high thermal stability for accurate creep measurements

> High resolution and low noise floor

//// CONCLUSION

No other Nanoindenter on the market is capable of such large indent matrices in such short periods of time, and with such stability!

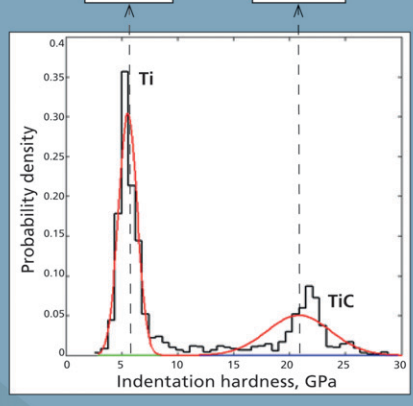

CSM Instruments | 197 1st Ave, suite 120 | Needham, MA 02494
Phone : 781-444-2250 | usinfo@csm-instruments.com | www.csm-instruments.com

Nanoindentation analysis as a two-dimensional tool for mapping the mechanical properties of complex surfaces

Nicholas X. Randall[a)]
CSM Instruments, Needham, Massachusetts 02494

Matthieu Vandamme[b)] and Franz-Josef Ulm
Department of Civil and Environmental Engineering, Massachusetts Institute of Technology, Cambridge, Massachusetts 02139

(Received 30 July 2008; accepted 11 December 2008)

Instrumented indentation (referred to as nanoindentation at low loads and low depths) has now become established for the single point characterization of hardness and elastic modulus of both bulk and coated materials. This makes it a good technique for measuring mechanical properties of homogeneous materials. However, many composite materials are composed of material phases that cannot be examined in bulk form ex situ (e.g., carbides in a ferrous matrix, calcium silicate hydrates in cements, etc.). The requirement for in situ analysis and characterization of chemically complex phases obviates conventional mechanical testing of large specimens representative of these material components. This paper will focus on new developments in the way that nanoindentation can be used as a two-dimensional mapping tool for examining the properties of constituent phases independently of each other. This approach relies on large arrays of nanoindentations (known as grid indentation) and statistical analysis of the resulting data.

I. INTRODUCTION

The nanoindentation method for assessing mechanical properties at low loads and shallow depths is well established for the characterization of thin films as well as bulk materials. The depth-sensing indentation method produces a load-displacement curve from which quantitative property values (commonly hardness and elastic modulus) can be calculated using a variety of approaches.[1–3] Although nanoindentation has proved to be a powerful technique for measuring the properties of homogeneous, monolithic material systems, little work has been done in optimizing the method for use on heterogeneous (composite) materials, of which most solids are made up.

It has already been shown that nanoindentation can be a valid tool for measuring the mechanical properties of small grains (grain size < 10 μm) within a composite matrix,[4] but such measurements have significant disadvantages, namely:

(i) A compromise always has to be made between having sufficient indentation depth to overcome surface roughness (most microstructures are polished in some way), but shallow enough depth to measure grain-only properties.

(ii) Most microstructures are mechanically polished, a process that can significantly work-harden the material in the near-surface region (particularly in metals) meaning that near-surface indentations may overestimate the actual hardness of a particular feature.

(iii) Many metallic microstructures are etched with acids to better observe their features under the optical microscope. Such etching can cause significant surface roughness as well as chemical modification of the near-surface region.

(iv) When indenting single grains, the indentations must be large enough to be visible by microscopy, otherwise the location cannot be verified.

(v) Individual phases are not always visible by microscopy, or no suitable etchant is available.

(vi) Indentation of a single grain may not give the properties of the grain only: the surrounding matrix may be softer than the grain, meaning that there may always remain an elastic component from the underlying substrate, even if the indentation depth is orders of magnitude less than the grain size.

(vii) When indenting single grains, it is impossible to know the depth of the grain below the surface, so even a relatively shallow indent may be sensing the substrate properties.

In addition to the aforementioned disadvantages of indenting single grains, the location of the indenter onto the grain may require significant time and the results obtained may have a large standard deviation owing to

[a)]Address all correspondence to this author.
e-mail: nra@csm-instruments.com
[b)]Present address: Université Paris-Est, Ecole des Ponts, UR Navier, 77455 Champs-sur-Marne, France
DOI: 10.1557/JMR.2009.0149

some of the factors already mentioned. This makes discrete nanoindentation a rather cumbersome tool for measuring the properties of single grains. Some classes of materials, particularly geomaterials (concretes, shales), cannot be easily polished owing to the significant mismatch in properties between their constituent phases. The resultant high surface roughness variations cause large statistical deviations in indentation results and therefore large numbers of indentations are required to obtain a reproducible value of hardness or elastic modulus. The recent study of such cementitious materials[5–7] resulted in the development of a novel grid indentation technique[7–12] which not only can be used to obtain key mechanical properties of heterogeneous materials at a particular length scale, but also can provide access to the volume fractions of independent phases. The objective of this paper is to use the grid indentation technique and apply it to a range of different multiphase materials and investigate whether the technique could become an accurate method of obtaining both quantitative and qualitative information about the morphology and mechanical properties of individual phases comprising the material.

II. THEORETICAL CONSIDERATIONS

A. Specifics of the grid indentation technique

Consider a material to be composed of two phases of different mechanical properties and characterized by a length scale D, as described in Fig. 1. If the indentation depth is much smaller than the characteristic size of the phases, $h \ll D$, then a single indentation test gives access to the material properties of either phase 1 or phase 2. If, in addition, a large number of tests is carried out on a grid (or matrix) defined by a grid spacing L that is larger than the characteristic size of the indentation impression, so as to avoid interference in between individual indentation tests, and much larger than the characteristic size of the two phases, then the probability of encountering one or the other phase is equal to the surface fraction occupied by the two phases on the indentation surface. On the other hand, an indentation test performed to a maximum indentation depth that is much larger than the characteristic size of the individual phases, $h \gg D$, senses the average response of the composite material, and the properties extracted from such an indentation experiment are representative in a statistical sense of the average properties of the composite material.

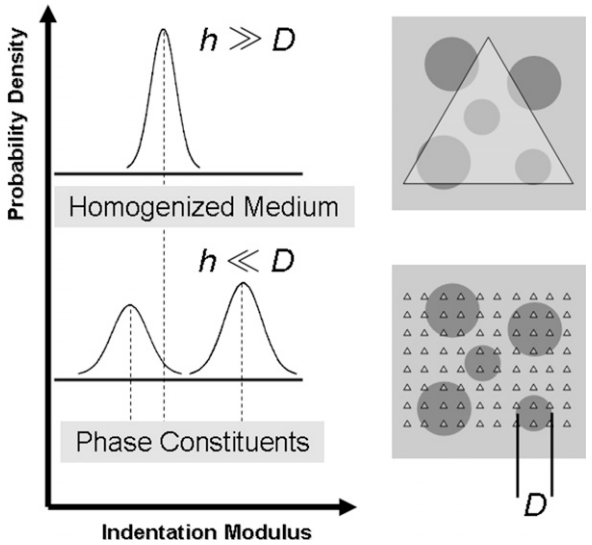

FIG. 1. Schematic of the principle of the grid indentation technique for heterogeneous materials. Small indentation depths allow the determination of phase properties, while larger indentation depths lead to the response of the homogenized medium (adapted from Constantinides et al., see Ref. 8).

If the characteristic size of the heterogeneity (e.g., the particle size) is denoted by D then it is useful to determine the characteristic size d_s of the material volume that is activated by the indentation test on the multiphase material. This size, d_s, can be roughly associated with a half-sphere projected underneath the indenter, similar to the iso-values of the resultant stress field. The indentation response will depend mostly on the material within a distance d_s from the indenter tip. If $d_s < D$ then the indentation test may probe only one phase and therefore characterize its intrinsic phase properties.

The size d_s of the volume of material probed by the indentation test depends on the indentation depth, h, on the geometry of the indenter (e.g., half-cone angle θ of a Berkovich indenter), on the properties of the indented material (indentation modulus, M, Poisson's ratio, ν, hardness, H, friction angle, α) and on the characteristic size of the heterogeneity, D. A straightforward dimensional analysis of the problem yields:

$$\frac{d_s}{h} = \Pi_{d_s}\left(\theta, \frac{M}{H}, \nu, \alpha, \frac{h}{D}\right) \quad . \tag{1}$$

The first four invariants are material properties (eventually of the composite material), while the last invariant, h/D, links the indentation depth to a characteristic scale, the characteristic size of the heterogeneity. In the case where $h/D \to 0$, this invariant skips out of the set of dimensionless quantities, giving:

$$h/D \to 0 \Rightarrow d_s \propto h \quad . \tag{2}$$

In this case, h is the sole length scale in the infinite half-space and the problem respects the condition of self-similarity. The indentation properties (M, H) extracted with a test where $h \ll D$ are representative of the elasticity and strength properties of the phase of size D. In contrast, the properties extracted with a test $h/D \gg 1$ sample the composite response. This can be illustrated by the example shown in Fig. 2 which

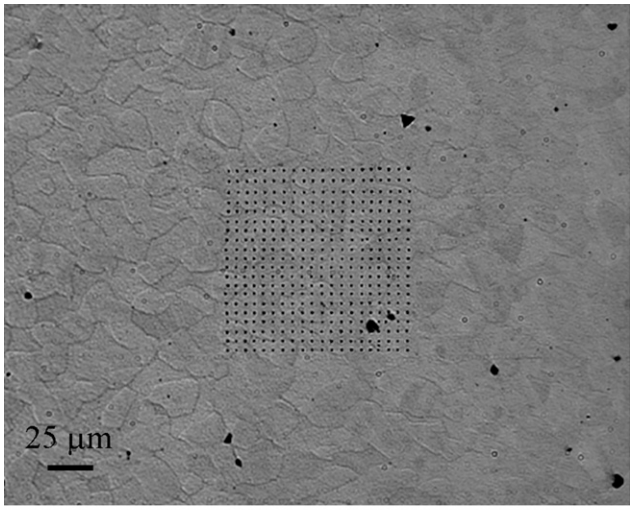

(a)

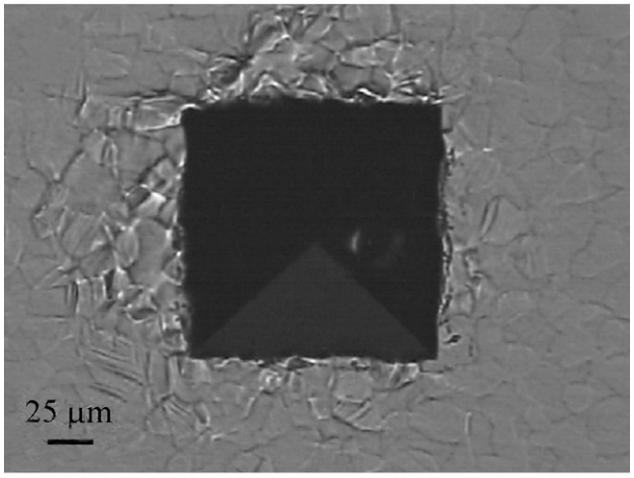

(b)

FIG. 2. Practical example of indentation of a polished α-β brass (naval brass CDA 464) microstructure that contains two phases of average grain size ~24 μm. Both micrographs are at the same magnification (200×). The grid indentation matrix in (a) contains 400 nanoindentations with 2 mN maximum load whereas (b) shows a single microindentation with 20 N maximum load.

shows the two aforementioned extremes: the grid indentation matrix in Fig. 2(a) contains 400 nanoindentations with 2 mN maximum load whereas Fig. 2(b) shows a single microindentation with 20 N maximum load. The material is a polished α-β brass (naval brass CDA 464) microstructure, which contains two phases of average grain size ~24 μm. In the former case, $h/D \approx 0$ (phase property differentiation); in the latter case, $h/D \approx 1$ (composite response). Note that a Berkovich geometry indenter was used for the grid matrix in Fig. 2(a) and a Vickers geometry indenter for the microindentation in Fig. 2(b).

The classical tools of instrumented indentation can therefore be extended to heterogeneous materials through a careful choice of the indentation depth, which will depend on the size of the elementary components. In addition to a large array of indentation tests, the statistical analysis will require subsequent statistical deconvolution of the indentation results. The choice of a critical depth, h_{crit}, below which intrinsic phase properties can reliably be measured by indentation has been studied both analytically and numerically.[8] Numerical simulations by Durst et al.[13] have focused on the measurement of indentation hardness by conical indentation on (almost) rigid perfectly plastic biphasic systems. Their simulations show that, if the contact radius $a < 0.7\ D$, then the indentation hardness of the indented phase is correctly measured. In addition, their conclusion was that this criterion is almost the same for a particle embedded in a matrix and a thin film on a substrate; that is, h_{crit} is almost independent of the shape of the indented phase and depends only on its characteristic size D. However, a reliable measurement of the indentation modulus may require a more stringent criterion, since the material volume that is solicited elastically below the indenter is much larger than the volume solicited plastically. In practice, this means that attempting to specifically indent a phase of interest is likely to fail since an optical image of a microstructure is only a two-dimensional representation of a three-dimensional structure. Another phase may be present just below the surface resulting in a composite response to the measured indentation. For a hard grain surrounded by a softer phase, such a composite response will yield an underestimated value for the modulus of the grain. Such a composite response and thus the influence of the softer surrounding phase can be minimized, however, by decreasing the depth of the indentations.[14] This observation reinforces the grid indentation technique as a far better method of addressing such issues.

A grid indentation array consists of a large number of indentations performed at random locations on the surface of a multiphase material. The indentations are shallow enough to ensure that the criterion $h/D < 0.1$ is respected, this being the critical h/D ratio below which the elastic properties of the indented composite do not diverge more than 10% from the elastic properties of the phase.[8,12] Although a few indentations may measure a composite response, this criterion ensures that a large majority of the indentations will probe the intrinsic properties of the individual phases. The experimental results can easily be displayed as histograms (or frequency plots) of the measured indentation properties (indentation hardness, H, indentation modulus, M, etc.), which in the case of a two-phase composite material display two peaks. The mean value of each peak represents the mean phase property. The area below each curve of the histogram is a measure of the percentage of all indentations performed on the corresponding phase, and is therefore a measure of the surface fraction of each phase. For a

perfectly disordered material, surface fractions and volume fractions are identical, meaning that the volume fraction of each phase of a heterogeneous material can also be obtained by an analysis of the experimental frequency plot. The combination of mechanical properties of phases with their volume fractions makes this method particularly appealing.

The randomness of the location of the indentations ensures that the measured properties are not correlated from indentation to indentation. If the indented material is perfectly disordered, this zero correlation can also be ensured by performing the indentations on a grid, as long as the spacing between indentations is greater than the characteristic size D of the phases. Since it is easier to program an indentation instrument to perform indentations on a grid, the approach is referred to as the "grid-indentation technique."[8] An additional advantage of programming an equispaced grid of indentations is that the measured values of a certain property (e.g., hardness) can be plotted as a three-dimensional map, where each "pixel" of the map corresponds to one load-depth indentation cycle. In this way, the surface of the material can be mapped in terms of its mechanical properties and correlated with microscopical observation. Such mapping of mechanical properties can also be performed with an atomic force microscope (AFM),[15,16] even though, due to calibration issues, AFM-based techniques may prove not as quantitative as nanoindentation-based ones for the measurement of an elastic modulus.

Although much of this explanation of the technique focuses on a two-phase composite for simplicity, it obviously applies to more phases as well, provided they exhibit sufficient contrast (mismatch) in their properties. To ensure repeatability of the technique, the analysis of the frequency plot, called the deconvolution technique, needs to be automated.

B. Deconvolution technique

In its original development[8,12] the deconvolution technique was carried out manually by fitting a number of probability density functions (PDF) to the experimental frequency plot (normalized histogram) of the measured quantity, making the deconvolution results dependent on the operator. More recently, Vandamme and Ulm[11] showed that an automated process can be successfully utilized to extract mean property values, volume fractions, and standard deviations of the phase mechanical properties. Although a full explanation of this process is beyond the scope of this paper, some points are helpful in understanding the methodology.

The first point that needs to be addressed is the best choice of distribution function for each peak in the frequency plot, the distribution function being uniquely defined by its statistical moments. If the measurements and the material were perfect, then for infinitely shallow indentations one would expect the peaks to be infinitely sharp, each peak being characterized by its first moment (mean value) only. In practice, however, there are several reasons for which the peaks of the histogram are not infinitely sharp, therefore requiring the use of moments of higher order:

(i) The measurements exhibit some noise which is considered as random and creates a spread of peaks, but no asymmetry.

(ii) Each phase has its own intrinsic variability, also causing a spread of the peaks.

(iii) The indentations are not infinitely shallow: even for an ideal material and ideal measurements, due to their finite depth, some indentations will mechanically solicit two (or more) phases simultaneously, resulting in a composite property.

For the sake of simplicity, the distribution is chosen so that all standardized central moments of order higher than the second are zero, this being a Gaussian distribution.

The deconvolution begins with the generation of the experimental cumulative distribution function (CDF), where N is the number of indentation tests performed on a specimen and $\{X_i\}_{i=1\ldots N}$ the sorted values of the measured property which is to be deconvoluted. This parameter can be the indentation modulus, M, the indentation hardness, H, or any other property obtained from the indentation test (creep properties, packing density, etc.). The N points of the experimental CDF of X, denoted by D_X, are obtained from:

$$D_X(X_i) = \frac{i}{N} - \frac{1}{2N}; \text{for } i \in [1;N] \quad . \tag{3}$$

It is assumed that the heterogeneous material is composed of n material phases with sufficient contrast in mechanical phase properties. The j-th phase occupies a volume fraction f_j of the indented surface. The best choice for the distribution of the mechanical properties of each phase is a Gaussian distribution, identified by its mean value μ_j^X and its standard deviation s_j^X. The CDF of the j-th Gaussian distributed phase is given by:

$$\min \sum_{i=1}^{N} \sum_{X} \left(\sum_{j=1}^{n} f_j D\left(X_i; \mu_j^X, s_j^X\right) - D_X(X_i) \right)^2 \quad . \tag{4}$$

To ensure that phases have sufficient contrast in properties, and to avoid the case where two neighboring Gaussians overlap, the optimization problem is additionally constrained by:

$$\mu_j^X + s_j^X \leq \mu_{j+1}^X - s_{j+1}^X \quad . \tag{5}$$

The volume fractions of the different phases sum to one. In addition to identifying the phase properties of heterogeneous materials, by careful choice of indentation depth

such that $h/D < 1/10$, it is also possible to link the scale of shallow indentation ($h/D \ll 1$) with the indentation properties at the composite scale ($h/D \gg 1$) without performing an actual indentation test at the composite scale. In other words, the grid indentation technique allows the mechanical properties of the phases within a composite material to be reconstituted into a composite (bulk) value. This process is explained in the following section.

C. Self-consistent indentation technique for the estimation of the homogenized indentation modulus

For small volumes of heterogeneous materials, it is often not possible to perform indentations that are deep enough to yield the bulk mechanical properties of the volume of interest. In this section we present a technique which, when applied to a grid of nanoindentations, enables the estimation of such bulk properties. In addition, the technique here presented to estimate bulk properties can be used as a tool for materials design: based on a grid of nanoindentations performed, a materials scientist can now "tweak" the properties of one constituent phase and immediately calculate the potential impact of this modification on the bulk property.

Consider a large array of indentation tests that satisfy the condition $h/D < 1/10$. In these tests, a heterogeneous data set of indentation moduli $\{M_i\}_{i=1,N}$ is determined that is representative of the heterogeneities of the multiphase material. The question we want to address analytically is: What is the corresponding homogenized indentation modulus M^{hom} that would be measured in indentation tests operated to $h/D \gg 1$? The problem is treated in the framework of linear micromechanics.[17]

1. Virtual composite material

The fundamental idea of the micromechanics approach developed below is that each test performed at a scale $h/D < 1/10$ is representative of a material phase, so that N indentation tests define a "virtual" composite material, which is composed of N phases characterized by N indentation moduli $\{M_i\}_{i=1,N}$ (Fig. 3). From the variational bounds of linear elasticity, it is known that the stiffness of the composite is situated between the Reuss bound (uniform stress) and the Voigt bound (uniform strain), which for a constant Poisson's ratio for all phases equally apply to the indentation modulus:

$$\left(\frac{1}{N}\sum_{(N)}\frac{1}{M_i}\right)^{-1} \leq M^{\text{hom}} \leq \frac{1}{N}\sum_{(N)} M_i \quad . \tag{6}$$

The focus of the micromechanics approach is to refine these estimates by considering the interaction between highly heterogeneously distributed phases. In this sense, M^{hom} can be viewed as the homogenized indentation modulus of the virtual composite material composed of N randomly distributed phases in the material.

2. Self-consistent micromechanics model

The inputs of the micromechanics model are:

(i) The volume fraction of each phase, $\varphi_i = 1/N$,

(ii) The elastic properties of each phase, given by the measured indentation modulus M_i, and Poisson's ratio ν_i, so that the bulk modulus K_i and shear modulus G_i read:

$$\begin{aligned} K_i &= \frac{E_i}{3(1-2\nu_i)} = \frac{1-\nu_i^2}{3(1-2\nu_i)} M_i \\ G_i &= \frac{E_i}{2(1+\nu_i)} = \frac{1-\nu_i}{2} M_i \quad . \end{aligned} \tag{7}$$

(iii) The morphology of the virtual composite. Given that each virtual phase occupies a volume fraction $\varphi_i = 1/N$ only, no phase can reasonably play the role of a matrix. In contrast, a polycrystal morphology seems particularly well-suited. The self-consistent scheme yields particularly good estimates for a polycrystal morphology, for which it was in fact initially developed.[18,19]

Using these elements and considering a spherical morphology for each virtual phase, an estimate of the homogenized indentation modulus of the virtual composite material is obtained in the isotropic case with[17]:

$$\begin{aligned} K^{\text{hom}} \left[\sum_{i=1}^{N} \frac{1}{K^{\text{hom}} + \alpha^{\text{hom}}(K_i - K^{\text{hom}})}\right] &= \sum_{i=1}^{N} \frac{K_i}{K^{\text{hom}} + \alpha^{\text{hom}}(K_i - K^{\text{hom}})} \\ G^{\text{hom}} \left[\sum_{i=1}^{N} \frac{1}{G^{\text{hom}} + \beta^{\text{hom}}(G_i - G^{\text{hom}})}\right] &= \sum_{i=1}^{N} \frac{G_i}{G^{\text{hom}} + \beta^{\text{hom}}(G_i - G^{\text{hom}})} \quad . \end{aligned} \tag{8}$$

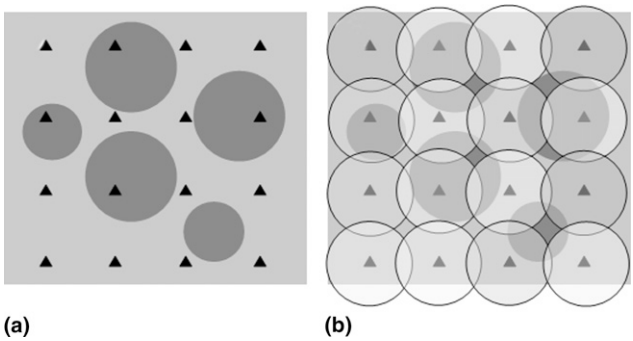

FIG. 3. (a) Grid of indentations performed on a multi-phase material and (b) associated virtual N-phase material. N is the number of indentations performed.

where:

$$\alpha^{\mathrm{hom}} = \frac{3K^{\mathrm{hom}}}{3K^{\mathrm{hom}} + 4G^{\mathrm{hom}}}$$
$$\beta^{\mathrm{hom}} = \frac{6}{5}\frac{K^{\mathrm{hom}} + 2G^{\mathrm{hom}}}{3K^{\mathrm{hom}} + 4G^{\mathrm{hom}}} \quad .$$

The equations in Eq. (8) are nonlinear, because of the coupling introduced by α^{hom} and β^{hom}. For large N, Eq. (8) cannot be solved analytically, but can easily be solved numerically (e.g., with Matlab). Then, M^{hom} is calculated from:

$$M^{\mathrm{hom}} = 4G^{\mathrm{hom}}\frac{3K^{\mathrm{hom}} + G^{\mathrm{hom}}}{3K^{\mathrm{hom}} + 4G^{\mathrm{hom}}}. \qquad (9)$$

3. Effect of the set of virtual Poisson's ratio on estimated homogenized indentation modulus

The sole nonexperimental input of the approach is a set of Poisson's ratio $\{\nu_i\}_{i=1,N}$ of the N virtual phases. The effect, which this set has on the homogenized indentation modulus M^{hom}, is here investigated numerically. A set of $N = 400$ values $\{M_i\}_{i=1,N}$, chosen randomly between 0 and 100 GPa, is generated. It is instructive to note that the Reuss-Voigt bounds [Eq. (6)] for $N\rightarrow\infty$ random realizations between 0 and $M_{\max}$ read:

$$0 = \lim_{N\rightarrow+\infty}\left(\frac{1}{N}\sum_{i=1}^{N}\frac{1}{i/N}\right)^{-1} \leq \frac{M^{\mathrm{hom}}}{M_{\max}} \leq \lim_{N\rightarrow+\infty}\left(\frac{1}{N}\sum_{i=1}^{N} i/N\right) = \frac{1}{2} \quad . \qquad (10)$$

To study the effect of Poisson's ratio, the following cases are investigated:

(i) Poisson's ratio ν_i is assumed the same in all N phases. For each ν_i, Eq. (8) is solved numerically with Matlab. Figure 4 displays the results of the calculation. The homogenized Poisson's ratio ν^{hom} is roughly equal to the Poisson's ratio ν_i of the virtual phases. In contrast, the homogenized indentation modulus varies little with Poisson's ratio ν_i, $M^{\mathrm{hom}}/M_{\max} = 0.415 \pm 1.5\%$.

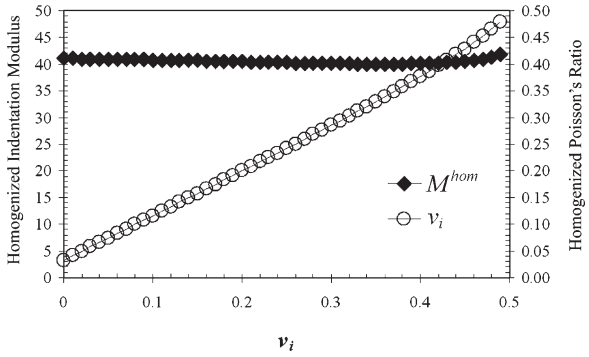

FIG. 4. Effect of a constant Poisson's ratio ν_i (assigned to 400 virtual phases) on the homogenized indentation modulus M^{hom} (black diamonds, left axis) and on the homogenized Poisson's ratio ν^{hom} (black circles, right axis).

(ii) Poisson's ratios $\{\nu_i\}_{i=1,N}$ are assumed to be uniformly distributed over [0,0.5]. 100 sets are generated, and for each set Eq. (8) is solved numerically. The homogenized indentation modulus varies little for the 100 numerical solutions, $M^{\mathrm{hom}}/M_{\max} = 0.415 \pm 0.3\%$.

The case studies show that the Poisson's ratios $\{\nu_i\}_{i=1,N}$ assigned to the phases have little effect on the homogenized indentation modulus M^{hom}, which deviates significantly from the Reuss-Voigt bounds [Eq. (6)]. The set of a constant Poisson's ratio $\nu_i = 0.2$ is chosen, since it provides a most convenient way to reduce the set of Eq. (8) to one single equation:

$$\sum_{i=1}^{N}\frac{1}{1+\frac{1}{2}(M_i/M^{\mathrm{hom}}-1)} = \sum_{i=1}^{N}\frac{M_i/M^{\mathrm{hom}}}{1+\frac{1}{2}(M_i/M^{\mathrm{hom}}-1)} \quad . \qquad (11)$$

This equation can easily be solved numerically and provides a simple way to estimate, from a set of indentation moduli $\{M_i\}_{i=1,N}$ measured with a grid of indentations, the homogenized indentation modulus M^{hom}.

III. EXPERIMENTAL PROCEDURE

To validate the aforementioned approach, four different composite materials were chosen to illustrate various different aspects of the method and its applicability to significantly different classes of materials. A summary of these chosen materials and the exact grid indentation parameters used in each case is as follows:

(i) Naval brass (CDA 464): brass of composition Cu-39.2 Zn-0.8 Sn, containing two primary phases, α and β, whose mechanical properties are known to be very similar and indistinguishable by standard microindentation techniques. Microstructure polished down to 0.05 μm alumina finish to reduce local work hardening in the near-surface region to a minimum. Average grain size is approximately 24 μm. Grid indentation array of 20 × 20 indents (total 400), maximum load 2 mN, 15 s pause at maximum load and separation between indents of 5 μm.

(ii) Cast iron: Graphite nodules in a tempered martensitic matrix. Heat treated by austenitizing, oil quenching and tempering. Composition in wt%: Fe, 3.52% C, 2.51% Si, 0.49% Mn, 0.15% Mo, 0.31% Cu. Grid indentation array of 30 × 30 indents (total 900), maximum load 5 mN, 10 s pause at maximum load and separation between indents of 5 μm.

(iii) Ti64-10TiC Alloy: Titanium alloy with matrix composition in wt% of 6% Al and 4% V, containing 10% TiC particles. Grid indentation array of 40 × 40 indents (total 1600), maximum load 5 mN, 5 s pause at maximum load and separation between indents of 3 μm.

(iv) M3 High speed steel: The microstructure consists of primary carbides distributed in a martensitic matrix and quantitative analysis by wavelength dispersive spectroscopy shows that two types of carbide are present, namely MC (where M is V or Cr) and M_6C (where M is Fe, W, Mo, Cr, or V). Grains of MnS are also present in the Fe matrix, having been included as a means of solid lubrication. The MC carbides are globular and dark colored, the M_6C carbides are angular and lighter colored, and the MnS grains are globular but smaller and pale colored. The microstructure is polished down to 0.25 μm alumina finish and etched in Nital (4% nitric acid and ethanol). This material was chosen to investigate whether the grid indentation technique can resolve four distinct phases. The grid indentation array is of 50 × 50 indents (total 2500), maximum load 5 mN, 5 s pause at maximum load and separation between indents of 3 μm.

The instrument used for all nanoindentation was a CSM Instruments Nanoindentation Tester (CSM Instruments, Needham, MA) with a Berkovich diamond indenter, this instrument being capable of large arrays of preprogrammed indentations (>1000) in a short timeframe. In standard operation, this machine is capable of making a grid array of 2500 indentations continuously over a period of 3–4 days. The large volume of resultant data is then exported, plotted as histograms, and deconvoluted to extract property and volume fraction information. In addition, the data can be plotted as a three-dimensional map. In all cases, the loading rate was set to provide a 30 s loading and a 30 s unloading cycle. All indentation testing was performed in compliance with ISO 14577, as was the subsequent calculation of indentation hardness and elastic modulus.[20]

IV. RESULTS

The results of the grid indentation array on the naval brass are summarized in Fig. 5. This material contains two phases (α and β respectively) with an approximate grain size of 24 μm. The grid of 400 indentations [Fig. 5(a)] covers an area of 100 × 100 μm which therefore includes approximately 16 grains and so provides sufficient coverage to resolve statistically different mechanical properties between phases.

The rough outlines of specific grains can be resolved in the grid indentation maps shown in Figs. 5(b) and 5(d) which represent hardness and elastic modulus, respectively. Figure 5(c) shows average indentation load-depth curves for each phase superimposed on the same axes: each curve represents the average of 100 indentations and provides adequate statistical separation between the α and β phases. The maximum indentation depths in the range 159–202 nm confirm that the criterion $h/D < 0.1$ is respected (in this particular case, $h/D = 0.008$). When plotted as histograms with $n = 2$, two distinct peaks appear as shown in Fig. 6. In the case of hardness, the first peak (α-phase) has a mean of 2.24 GPa, standard

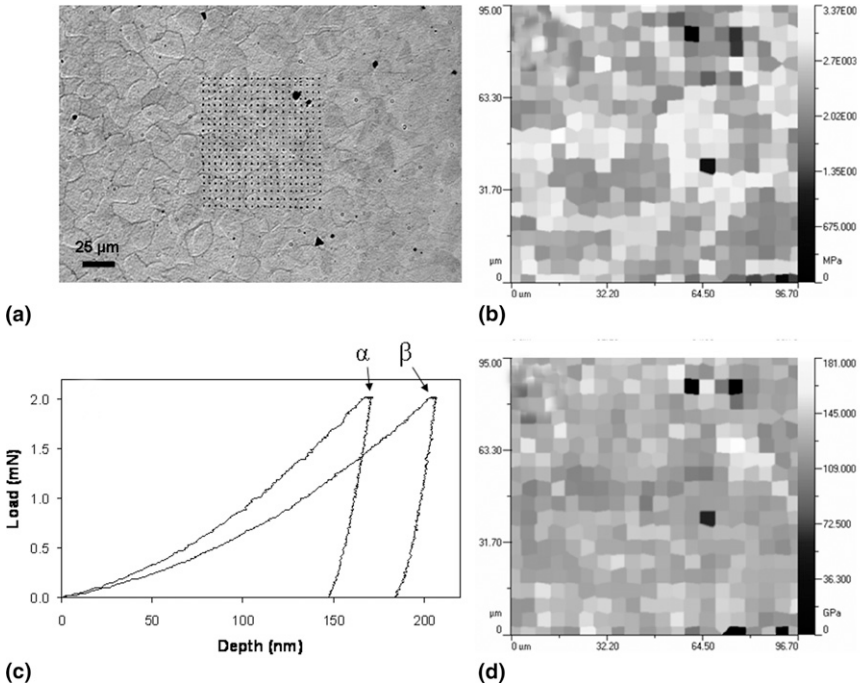

FIG. 5. Grid indentation array on polished α-β brass (naval brass CDA 464) microstructure, which contains two phases of average grain size ~24 μm. (a) Optical micrograph (200×) of 400 indent matrix with (b) corresponding hardness map, and (d) elastic modulus map. An example of a load-depth curve from each phase is shown in (c).

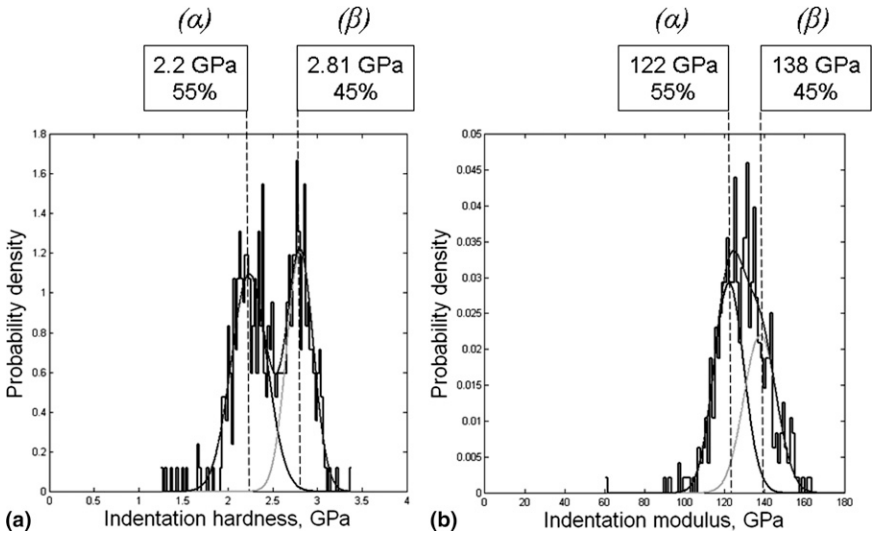

FIG. 6. Grid indentation histograms on polished α-β brass (naval brass CDA 464), showing the peaks for each of the two phases and the deconvoluted values of (a) hardness and (b) elastic modulus. Volume fraction percentages are shown in each case.

deviation of ±0.20 GPa, and volume fraction of 54.8%. The second peak (β-phase) has a mean of 2.81 GPa, standard deviation of 0.15 GPa, and volume fraction of 45.2%. In the case of elastic modulus, the two peaks are closer together, the first having a mean of 122.3 ± 7.5 GPa and the second a mean of 138.0 ± 8.2 GPa. Using these values, the reconstituted elastic modulus of the bulk is calculated as 128.7 GPa. This value was verified by making a set of 10 microindentations on the same material with a maximum applied load of 20 N and a Vickers indenter (same area-to-depth ratio as the Berkovich geometry used for the nanoindentation grid). An example of one such microindentation is shown in Fig. 2(b) and had a maximum indentation depth of 10.4 μm, giving a ratio h/D of 0.43. The measured indentation modulus of the bulk was 123.6 GPa which is an excellent correlation with the homogenized indentation modulus estimated at 128.7 GPa with Eq. (11). The Reuss bound was 128.0 GPa and the Voigt bound 129.3 GPa for the homogenized indentation modulus.

The results of the grid indentation array on the cast iron are summarized in Fig. 7. This material contains three phases (graphite, martensite, and carbide) and the grid of 900 indentations covers an area of 150 × 150 μm. The optical micrograph in Fig. 7(a) shows the exact area where the grid array was made. This area seems to contain an average quantity of dark colored spherical graphite particles.

The histograms plotted in Fig. 7 with $n = 3$ show three peaks. In the case of hardness, the first peak (graphite) has a mean of 0.78 ± 0.10 GPa and volume fraction of 5%. The second peak (martensite) has a mean of 3.5 ± 0.7 GPa and volume fraction of 70%. The third peak (carbide) has a mean of 5.7 ± 0.6 GPa and volume fraction of 25%. In the case of elastic modulus, the first peak has a mean of 68 ± 16 GPa, the second peak a mean of 204 ± 57 GPa, and the third peak a mean of 300 ± 27 GPa. The homogenized indentation modulus is estimated at 210 GPa with Eq. (11). The soft graphite phase has the most distinct peak, this being a significant mismatch with the iron matrix which is a composite of martensite and carbide. An average graphite particle diameter of 15 μm and maximum indentation depth of average 223 nm confirm that the criterion $h/D < 0.1$ is respected (in this particular case, $h/D = 0.015$). The volume fractions for the martensite and carbide are inaccurate in these deconvoluted results. It is known that this material contains approximately 5% graphite, 94% martensite, and 1% carbide. Therefore, a choice of $n = 3$ would be a correct assumption, but because the carbide percentage is so small, it gets swamped by the martensite peak and the volume fraction is significantly overestimated. For materials of this type, a deconvolution with $n = 2$ might provide a more accurate representation (in this case, $n = 2$ yields a hardness of 0.598 ± 0.207 GPa and volume fraction of 2.9% for graphite and a hardness of 3.81 ± 1.36 GPa and volume fraction of 97.1% for martensite).

The results of the grid indentation array on the Ti64-10TiC are summarized in Fig. 8. This material contains two phases (titanium and TiC) and the grid of 1600 indentations covers an area of 120 × 120 μm. The optical micrograph in Fig. 8(a) shows the exact area where the grid array was made and the two phases are clearly visible.

The histograms plotted in Fig. 8 with $n = 2$ show two peaks. In the case of hardness, the first peak (titanium) has a mean of 5.55 ± 0.83 GPa and volume fraction of 63.5%. The second peak (TiC) has a mean of 20.83 ± 2.89 GPa and volume fraction of 36.5%. In the case of

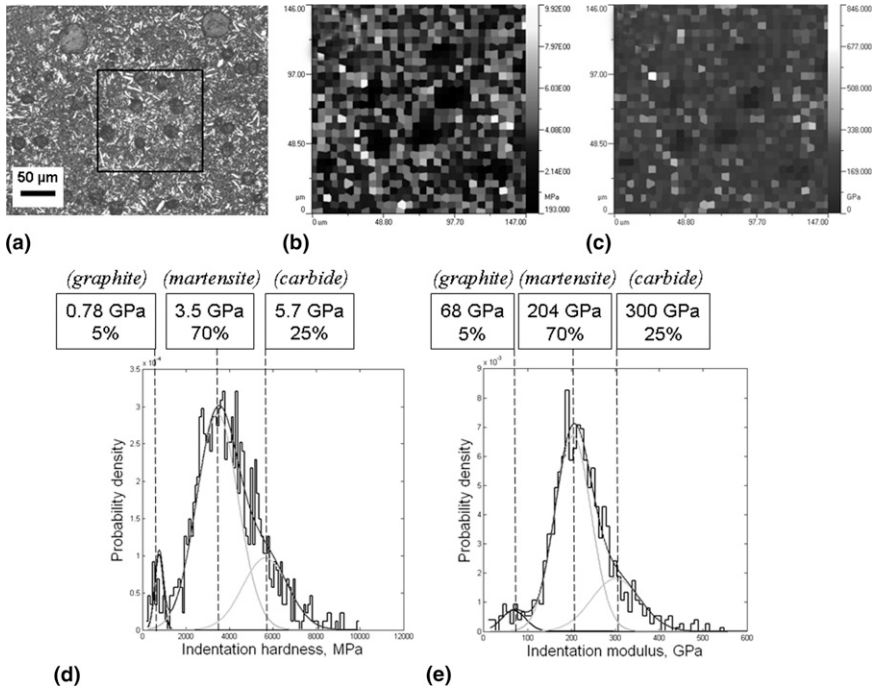

FIG. 7. Grid indentation array on cast iron microstructure, showing (a) optical micrograph (200×) of 900 indent matrix position, (b) hardness map, (c) elastic modulus map, (d) hardness histogram, and (e) elastic modulus histogram.

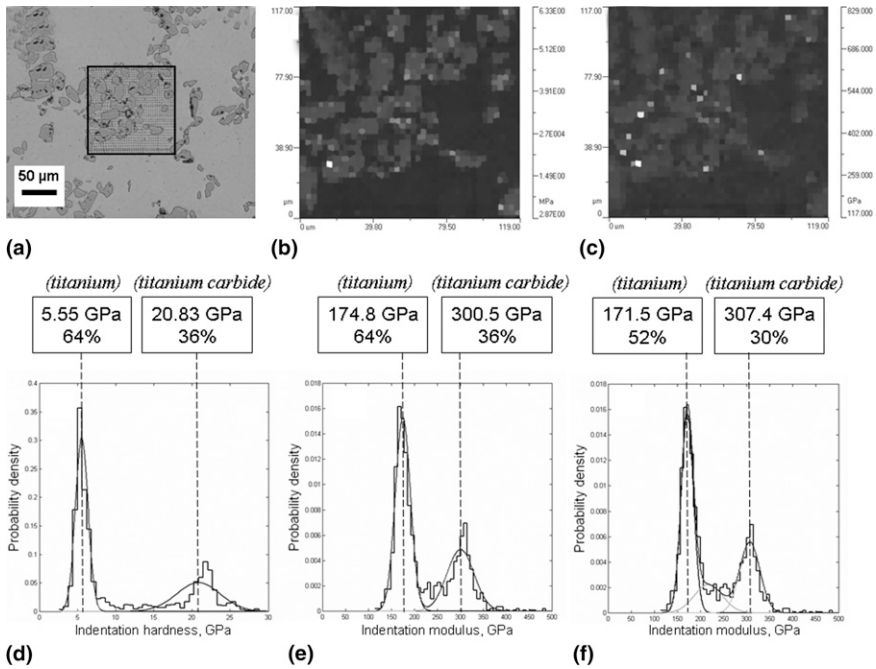

FIG. 8. Grid indentation array on Ti64-10TiC microstructure, showing (a) optical micrograph (200×) of 1600 indent matrix position, (b) hardness map, (c) elastic modulus map, (d) hardness histogram, (e) elastic modulus histogram (two-Gaussian), and (f) elastic modulus histogram (three-Gaussian).

elastic modulus, the first peak has a mean of 174.8 ± 16.6 GPa and the second peak a mean of 300.5 ± 29.9 GPa. The homogenized indentation modulus is estimated at 212.7 GPa with Eq. (11).

The results of the grid indentation array on the M3 high speed steel are summarized in Fig. 9. This material contains four main phases [iron (Fe) matrix, manganese sulphide (MnS), M_6C, and MC carbides] and the grid of

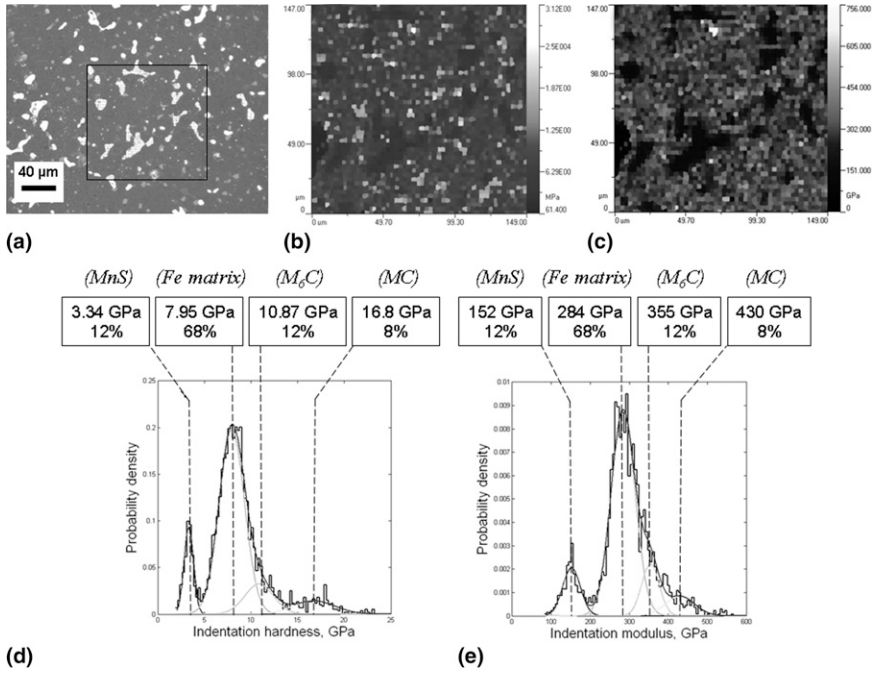

FIG. 9. Grid indentation array on M3 high-speed steel microstructure, showing (a) optical micrograph (200×) of 2500 indent matrix position, (b) hardness map, (c) elastic modulus map, (d) hardness histogram, and (e) elastic modulus histogram.

2500 indentations covers an area of 150 × 150 μm. The optical micrograph in Fig. 9(a) shows the exact area where the grid array was made and the four phases are clearly visible. A full explanation of the microstructure of this material is given in previous work by Randall et al.[4]

The histograms plotted in Fig. 9 with $n = 4$ show four peaks. The first peak (MnS) has a mean hardness of 3.34 ± 0.51 GPa, mean modulus of 152.1 ± 22.9 GPa, and volume fraction of 11.8%. The second peak (Fe matrix) has a mean hardness of 7.95 ± 1.37 GPa, mean modulus of 284.4 ± 30.7 GPa, and volume fraction of 67.7%. The third peak (M_6C carbide) has a mean hardness of 10.87 ± 1.55 GPa, mean modulus of 354.5 ± 22.6 GPa, and volume fraction of 12.6%. The fourth peak (MC carbide) has a mean hardness of 16.8 ± 2.24 GPa, mean modulus of 430.4 ± 37.4 GPa, and volume fraction of 7.9%. The homogenized indentation modulus is estimated at 279.7 GPa with Eq. (11). Considering that grain sizes vary in the range 4 μm (MC carbides) up to 15 μm (iron grains) and maximum indentation depths average 80 nm in the hardest carbides and 232 nm in the softest MnS grains confirms that the criterion $h/D < 0.1$ is respected (in this particular case, $0.015 \leq h/D \leq 0.020$).

V. DISCUSSION

The four composite materials analyzed in this study covered a broad range of mechanical properties and exhibited from two to four significantly different phases. In all cases the indentation results were analyzed both individually and globally, the former giving access to the mechanical properties of the indented region, the latter describing the composite material response. All grid indentation arrays were load-controlled, so the maximum indentation load was identical for all measurements within an array. The resultant indentation depths were therefore directly linked to the mechanical properties of individual phases and varied depending on whether the particular depth corresponded to a pure phase or an interaction between two or more phases. In all cases, the mechanical phases coincide with discrete chemical phases, meaning that the grid indentation technique provides a direct link between physical chemistry and mechanics. This is a direct consequence of the choice of indentation depth h, which was deliberately chosen to be small enough in relation to the characteristic length of the microstructural heterogeneities D. For all four sample materials tested, the criterion $h/D < 0.1$ was respected and so the mechanical properties of individual phases could be accurately resolved. However, in some cases where the characteristic length was of the same order of magnitude as the indentation depth, the criterion $h/D < 1$ was exceeded in a given number of indentations within the global array. Examples of this include some of the carbides in the M3 high speed steel where significant scatter in the measured properties was observed. In principle, a further reduction in the maximum indentation depth might overcome this experimental obstacle but the nanoindentation technique is currently limited by the sharpness of the three-sided pyramidal indenters used. With current diamond polishing methods, it is not possible to obtain highly accurate pyramidal geometries

for $h < 25$ nm. Even if such geometries were available, the measured property values at such depth scales would be plagued by discrepancies due to deviations from the perfect shape (indentation size effects) and from local surface modification (e.g., work hardening of the near surface region from polishing).

The volumetric proportions of all measured phases were reproducibly estimated from the relative areas of each individual Gaussian distribution under the cumulative frequency histograms. These proportions demonstrate the ability of the grid indentation technique to quantify the relative presence of different phases, although there are two important limitations that need to be addressed: the first is that such volume fractions are determined from the differential mechanical properties of the phases and not from their differential chemical composition; the second is that the typical total area of the grid indentation array ($\sim 10^3$ μm^2) remains only a small volumetric proportion of the bulk composite material. This means that volumetric proportions measured in this way are only meaningful if the area selected for grid indentation analysis contains similar proportions of individual phases as the bulk.

The sample materials with phases of similar elastic modulus (e.g., α-β brass) showed relatively low scatter and high repeatability, confirming the microstructural and mechanical homogeneity of the alloy and the robustness of the indentation experiments and analysis. Apart from the obvious case of the local response to an indentation being composite, the observed scatter in certain datasets could invariably be due to other factors such as:

(i) Surface roughness being of the same order of magnitude as the indentation depth, resulting in inconsistent contact area between indenter and material.

(ii) Imperfections in the microstructure (grain boundaries, porosity, contaminant inclusions, etc.).

(iii) Preferential polishing of the microstructure, resulting in certain phases being at different heights in relation to others.

(iv) Variations in surface mechanical properties as a direct result of polishing (work hardening, oxidation, etc.).

For materials containing phases with significantly different hardness, a common observation is that the harder phase exhibits a wider spread in its Gaussian distribution than the softer phase. This is due to the elastic response from the underlying material and can be seen best in Fig. 8(d) where the TiC peak is significantly more spread than that for the titanium. This effect is commonly observed, even for indentation depths two orders of magnitude smaller than the grain size, suggesting that the criterion $h/D < 0.1$ is not sufficient (or severe enough) in such cases. In contrast, the grid indentation technique seems to provide a better measure of the individual response of each phase for hardness because the calculation of hardness is based solely upon plastic deformation, whereas for the elastic modulus there is nearly always a composite response from all phases, even at very shallow indentation depths.

The results on all four measured sample materials (Figs. 5 and 7–9) are displayed as three-dimensional mechanical property maps where each "pixel" of the map corresponds to one load-depth indentation cycle. The direct correlation between the microstructure observed by optical microscopy and the corresponding mechanical property map proves that such mapping provides a means of characterizing the microstructure at the scale defined by the chosen indentation depth and the spatial distribution (defined by the separation between consecutive indents). In some cases, the mechanical property maps are able to display phase distribution even though the phases cannot be resolved by microscopy. This makes the technique particularly useful for measuring phases that may be below the surface, but still at a depth less than h.

Regarding the estimation of the homogenized indentation modulus, the following comments can be made:

(i) The Voigt and Reuss bounds are close to each other if the material is not heterogeneous (naval brass), but can yield a poor estimate if the material is made of constitutive phases whose properties are very different (M3 steel).

(ii) As expected, the homogenization scheme yields an estimate for the indentation modulus which is between the Reuss and the Voigt bounds.

(iii) The homogenization scheme yields an estimate for the indentation modulus that is much better than the Reuss and Voigt bounds.

This study would not be complete without an analysis of the relative effect of the number of phases n (which are presumed present in the material) on the deconvolution results. As an example, let us take the dataset for the Ti64-10TiC shown in Fig. 8, for which the hardness and elastic modulus histograms have been deconvoluted based on the condition $n = 2$. This is the most valid assumption as the material has been processed from two distinctly different precursor materials (titanium and titanium carbide) and both phases can be clearly distinguished by optical microscopy of the surface. Figure 8(e) shows the histogram for elastic modulus in which two very distinct peaks are visible. However, some additional overlapping data can also be seen between these two peaks. If the same dataset is deconvoluted with $n = 3$ then a third peak can be created (between the two main peaks) which "captures" all the overlapping data. In this way, the actual mean values of the two main peaks may be a more reliable estimate of the individual phase properties than if only a two-Gaussian distribution had been used. For the two-Gaussian case in Fig. 8(e), the first peak has a mean of 174.8 ± 16.6 GPa and the second peak a mean of 300.5 ± 29.9 GPa. For the three-Gaussian case in Fig. 8(f), the first peak has a mean of 171.5 ± 13.3 GPa

and the second peak a mean of 307.4 ± 21.9 GPa. Independent indentation experiments on pure titanium (E = 169.8 ± 7.4 GPa) and pure titanium carbide (E = 311.6 ± 18.9 GPa) confirm that the three-Gaussian distribution gives mean modulus values closer to the actual material properties, although the differences are not significant (<4%).

VI. CONCLUSIONS

The grid indentation technique has been proven as an excellent two-dimensional mapping tool for examining the properties of constituent phases independently of each other in composite material microstructures. More specifically, the method has the following attributes:

(1) Allows mean values of hardness and elastic modulus to be extracted for individual phases, as well as their volume fractions.

(2) Works very well for a wide range of multiphase materials (ceramics and metals).

(3) Peaks tend to be more distinct for hardness than modulus because the volume of material solicited plastically is smaller than that elastically.

(4) Easier to get individual response of each phase for hardness, whereas for modulus there is a composite response from all phases.

(5) Peaks can show more spread if the indented phase is much harder than the others, due to elastic response from underlying material (even with indentation depths two orders of magnitude smaller than the grain size!).

(6) Excellent correlation between the homogenized indentation modulus (estimated from a grid of nanoindentations) and the actual bulk indentation modulus (measured by instrumented microindentation).

(7) Simplified micromechanical approach can provide useful data for modeling.

Further optimization of this technique will allow in situ mechanical properties to be extracted at the micro- and nanoscales, providing a valid method of correlating individual phase properties with bulk response, and a powerful tool for materials characterization.

ACKNOWLEDGMENTS

The authors would like to thank George Vander Voort at Buehler for providing the naval brass, Robert Aharanov at Federal Mogul for providing the cast iron, and Susan Abkowitz at Dynamet Technology for providing the Ti64 alloy. The French Ministry of Public Works is acknowledged for its financial support which enabled M.V.'s doctoral studies at MIT.

REFERENCES

1. M.F. Doerner and W.D. Nix: A method for interpreting the data from depth-sensing indentation instruments. *J. Mater. Res.* **1,** 601 (1986).
2. J.L. Loubet, J.M. Georges, and G. Meille: Vickers indentation curves of elastoplastic materials, in *Microindentation Techniques in Materials Science and Engineering*, edited by P.J. Blau and B.R. Lawn (ASTM Intl., West Conshohocken, PA, 1986), p. 72.
3. W.C. Oliver and G.M. Pharr: An improved technique for determining hardness and elastic modulus using load and displacement sensing indentation experiments. *J. Mater. Res.* **7,** 1564 (1992).
4. N.X. Randall, R. Christoph, S. Droz, and C. Julia-Schmutz: Localized micro-hardness measurements with a combined scanning force microscope/nanoindentation system. *Thin Solid Films* **291,** 348 (1996).
5. G. Constantinides, F-J. Ulm, and K.J. Van Vliet: On the use of nanoindentation for cementitious materials. *Mater. Struct.* **36,** 191 (2003).
6. F-J. Ulm, G. Constantinides, and F.H. Heukamp: Is concrete a poromechanics material? A multiscale investigation of poroelastic properties. *Mater. Struct.* **37,** 43 (2004).
7. G. Constantinides and F-J. Ulm: The effect of two types of C-S-H on the elasticity of cement-based materials: Results from nanoindentation and micromechanical modeling. *Cem. Concr. Res.* **34,** 67 (2004).
8. G. Constantinides, K.S.R. Chandran, F-J. Ulm, and K.J. Van Vliet: Grid indentation analysis of composite microstructure and mechanics: Principles and validation. *Mater. Sci. Eng., A* **430,** 189 (2006).
9. G. Constantinides and F-J. Ulm: The nanogranular nature of C-S-H. *J. Mech. Phys. Solids* **55,** 64 (2007).
10. F-J. Ulm, M. Vandamme, C. Bobko, J.A. Ortega, K. Tai, and C. Ortiz: Statistical indentation techniques for hydrated nanocomposites: Concrete, bone, and shale. *J. Am. Ceram. Soc.* **90,** 2677 (2007).
11. M. Vandamme and F-J. Ulm: The nanogranular origin of concrete creep: A nanoindentation investigation of microstructure and fundamental properties of calcium-silicate-hydrates, CEE Report R08-01 (Department of Civil and Environmental Engineering, Massachusetts Institute of Technology, Cambridge, MA, 2008).
12. G. Constantinides and F-J. Ulm: Invariant mechanical properties of calcium-silicate-hydrates (C-S-H) in cement-based materials: Instrumented nanoindentation and microporomechanical modeling, CEE Report R06-01 (Department of Civil and Environmental Engineering, Massachusetts Institute of Technology, Cambridge, MA, 2006).
13. K. Durst, M. Goken, and H. Vehoff: Finite element study for nanoindentation measurements on two-phase materials. *J. Mater. Res.* **19,** 85 (2004).
14. A. Perriot and E. Barthel: Elastic contact to a coated half-space: Effective elastic modulus and real penetration. *J. Mater. Res.* **19,** 600 (2004).
15. D.C. Hurley, M. Kopycinska-Müller, A.B. Kos, and R.H. Geiss: Nanoscale elastic-property measurements and mapping using atomic force acoustic microscopy. *Meas. Sci. Technol.* **16,** 2167 (2005).
16. S.A. Asif, K.J. Wahl, R.J. Colton, and O.L. Warren: Quantitative imaging of nanoscale mechanical properties using hybrid nanoindentation and force modulation. *J. Appl. Phys.* **90**(3), 1 (2001).
17. L. Dormieux, D. Kondo, and F-J. Ulm: *Microporomechanics*, 1st ed. (John Wiley & Sons, New York, NY, 2006).
18. A.V. Hershey: The elasticity of an isotropic aggregate of anisotropic cubic crystals. *J. Appl. Mech.* **21,** 236 (1954).
19. E. Kröner: Calculation of the elastic constants of a polycrystal from the constants of the single crystal. *Z. Phys.* **151,** 504 (1958).
20. International Organization for Standardization: ISO 14577, Metallic materials—Instrumented indentation test for hardness and materials parameters (International Organization for Standardization, 2007).